Journal of Power Sources 204 (2012) 187–192

Contents lists available at SciVerse ScienceDirect

Journal of Power Sources

journal homepage: www.elsevier.com/locate/jpowsour

Short communication

Preparation and electrochemical properties of Co-doped and none-doped $Li[Li_xMn_{0.65(1-x)}Ni_{0.35(1-x)}]O_2$ cathode materials for lithium battery batteries

Zhaohui Tang, Zhixing Wang*, Xinhai Li, Wenjie Peng

School of Metallurgical Science and Engineering, Central South University, Changsha 410083, China

ARTICLE INFO

Article history:
Received 2 July 2011
Received in revised form 2 December 2011
Accepted 20 December 2011
Available online 29 December 2011

Keywords:
Cathode
Mn-based
Solid-state reaction
Electrochemical properties

ABSTRACT

Li-rich Mn-based Co-doped $Li[Li_xMn_{0.65*0.995(1-x)}Ni_{0.35*0.995(1-x)}Co_{0.005(1-x)}]O_2$ and none-doped $Li[Li_xMn_{0.65(1-x)}Ni_{0.35(1-x)}]O_2$ cathode materials were prepared by a conventional solid-state reaction. The initial charge and discharge test were carried out in the voltage ranges of 2.0–4.8 V and 2.0–4.6 V, then change to 3.0–4.3 V for cyclic test. XRD revealed that all the materials prepared show a (0 0 3) peak at $2\theta = 18.5^\circ$ as a main peak and clearly present a pure hexagonal structure. SEM characterization proved that the as prepared materials are constituted of small and homogenous particles. The Co-doped $Li[Li_{0.0909}Mn_{0.588}Ni_{0.3166}Co_{0.0045}]O_2$ sample expresses highest initial efficiency of 78.8% and highest energy density of 858.4 mWh g^{-1}, while the none-doped $Li[Li_{0.2308}Mn_{0.5}Ni_{0.2692}]O_2$ sample behaves lowest of 56.5% and 590.1 mWh g^{-1}. Furthermore, discharge capacity keeps on going up at the initial stage of cyclic process, which can reach the highest discharge capacity approximately in the fifth cycle. Almost no capacity loss is observed after 30 cycles.

1. Introduction

Recently, more and more interests have been focused on the complicated compositional cathode materials for lithium-ion batteries. The layered structure $LiMO_2$ (M = Co, $Ni_{0.8}Co_{0.95}Al_{0.05}$, $Ni_{0.33}Mn_{0.33}Co_{0.33}$, $Ni_{0.5}Mn_{0.3}Co_{0.2}$, etc.) materials have been widely used commercially for their high capacity, good thermal stability and excellent charge–discharge properties. Moreover, a series of lithium-rich Mn-based materials of $xLi_2MnO_3\cdot(1-x)LiMO_2$, where $LiMO_2$ has layered structure, M stands for Co, Ni, $Ni_{0.5}Mn_{0.5}$, or other transitional elements, have been extensively studied for their high capacity and good structure stability at high charged state [1–16]. It is also found that the valence state of Mn is +4 when the materials combined in the layered compounds, which is the key factor for the structure stability and electrochemical performance improvement of these composite compounds.

However, the problem of high charge voltage plateau and low efficiency in the initial cycle of Li_2MnO_3 or Li_2MnO_3-based materials obstruct their application greatly. The mechanism of the high charge voltage plateau of 4.5 V is not well-defined up to now. Johnson et al. reported that acid treatment can greatly lower the first-cycle inefficiency of the Li/Li_2MnO_3 cells, they considered a single phase formulated in two-component notation as $(1-x)Li_{2-\delta}H_\delta\cdot(x)MnO_2$ in which the oxygen array is common to both component; the manganese ions and some residual lithium ions remain in the octahedral sites of their original layer [1]. Yu et al. investigated phenomenon of increasing capacity of $0.65Li_2MnO_3$ 0.35 $Li(Ni_{1/3}Co_{1/3}Mn_{1/3})O_2$, the peak above 4.5 V appears in the first cycle and then decreasing gradually [11]. Lim et al. reported that $xLi_2MnO_3\cdot yLi[Ni_{1/3}Co_{1/3}Mn_{1/3}]O_2\cdot zLiNiO_2$ ($0.48 \le x \le 0.60$, $0.32 \le y \le 0.40$, $0 \le z \le 0.20$) samples have two distinguished voltage regions, of which the first voltage region below 4.45 V originated from the oxidation of transitional metal ions to tetravalent ion, the voltage plateau region locating in 4.45 V is mainly due to the electrochemical removal of Li_2O associated with irreversible loss of oxygen from the lattice [12]. Kang and Thackeray also considered that during the initial charge, oxygen loss occurs above 4.6 V accompanying with extraction of lithium from $xLi_2MnO_3\cdot(1-x)LiMO_2$ electrodes [15]. They viewed that Li–Ni–PO_4-coated treatment enhances the rate capability, but cannot lower the first-cycle charging plateau. Nevertheless, litter investigation focused on microelement doping and Li excess amount for Lithium rich Mn–Ni materials, especially for Mn:Ni = 0.65:0.35 system [17].

In this paper, Li-rich Mn-based Co-doped $Li[Li_xMn_{0.65*0.995(1-x)}Ni_{0.35*0.995(1-x)}Co_{0.005(1-x)}]O_2$ and none-doped $Li[Li_xMn_{0.65(1-x)}Ni_{0.35(1-x)}]O_2$ cathode materials were prepared to analysis effect of Co-doping and Li excessive. XRD, SEM and ICP test are investigated on the characteristics of the crystalline phase structure, morphology and physical composition. Electrochemical properties carried out in different voltage ranges were major investigated.

* Corresponding author. Tel.: +86 018684675178; fax: +86 0731 88836633.
E-mail address: tangzh106@163.com (Z. Wang).

0378-7753/$ – see front matter © 2011 Elsevier B.V. All rights reserved.
doi:10.1016/j.jpowsour.2011.12.040

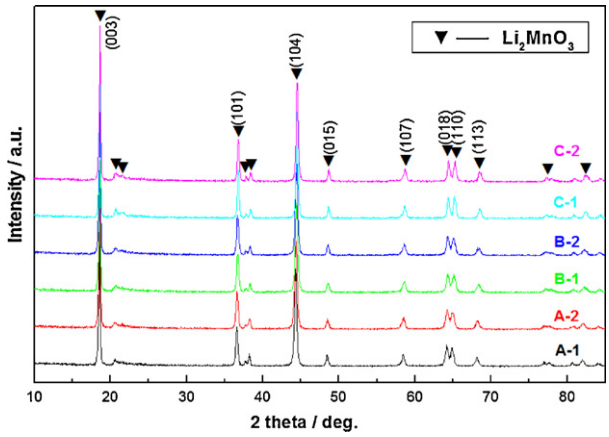

Fig. 1. XRD patterns of Co-doped $Li[Li_xMn_{0.65*0.995(1-x)}Ni_{0.35*0.995(1-x)}Co_{0.005(1-x)}]O_2$ and non-doped $Li[Li_xMn_{0.65(1-x)}Ni_{0.35(1-x)}]O_2$ samples (A–C referring to samples of $x = 0.0909, 0.1667, 0.2308$; -1 and -2 referring to Co-doped and none-doped).

2. Experiment

Materials were prepared by a conventional solid-state reaction using lithium carbonate and the metal hydroxide with Mn:Ni of 0.65:0.35 in mol ratio. In the meanwhile, 0.5 mol% (Co/[Mn, Ni and Co in all]) ultrafine Co_3O_4 powder was also added separately. To compare the effect of Co-doping, blank experiment were also carried out at completely the same synthesis condition. The pure phase can be prepared when Li excess value x keeps between 0.0909 and 0.2308 in our initial research works. Therefore, Li excess value x selected was 0.0909, 0.1667, and 0.2308, referring to code A-1, A-2, B-1, B-2, and C-1, C-2 for Co-doped and none-doped sample correspondingly. The materials were synthesized from lithium carbonate, the metal hydroxide, and ultrafine Co_3O_4 powder taken in stoichiometric quantities as the following procedure. (1) All ingredients were mixed for 3 h by ball-milling. (2) The mixture was calcinated at 900 °C in air for 20 h, and then cooled naturally. To find an optimized ratio, the samples were compared with a fixed calcination condition.

Powder X-ray diffraction (XRD, Rint-1000, Rigaku, Japan) using Cu Kα radiation was employed to identify the crystalline phase of the synthesized materials. XRD data were obtained ($2\theta = 10–85°$) with a step size of 0.02°. The particle size and morphology were measured by scanning electron microscopy (SEM, JSM6380LV) with an accelerating voltage of 20 kV. The composition in terms of transition metal contents in the materials were determined by the inductively coupled plasma (ICP, Thermo Electron Corporation).

The electrochemical characterizations were performed using CR2430 coin cells. For positive electrode fabrication, the prepared

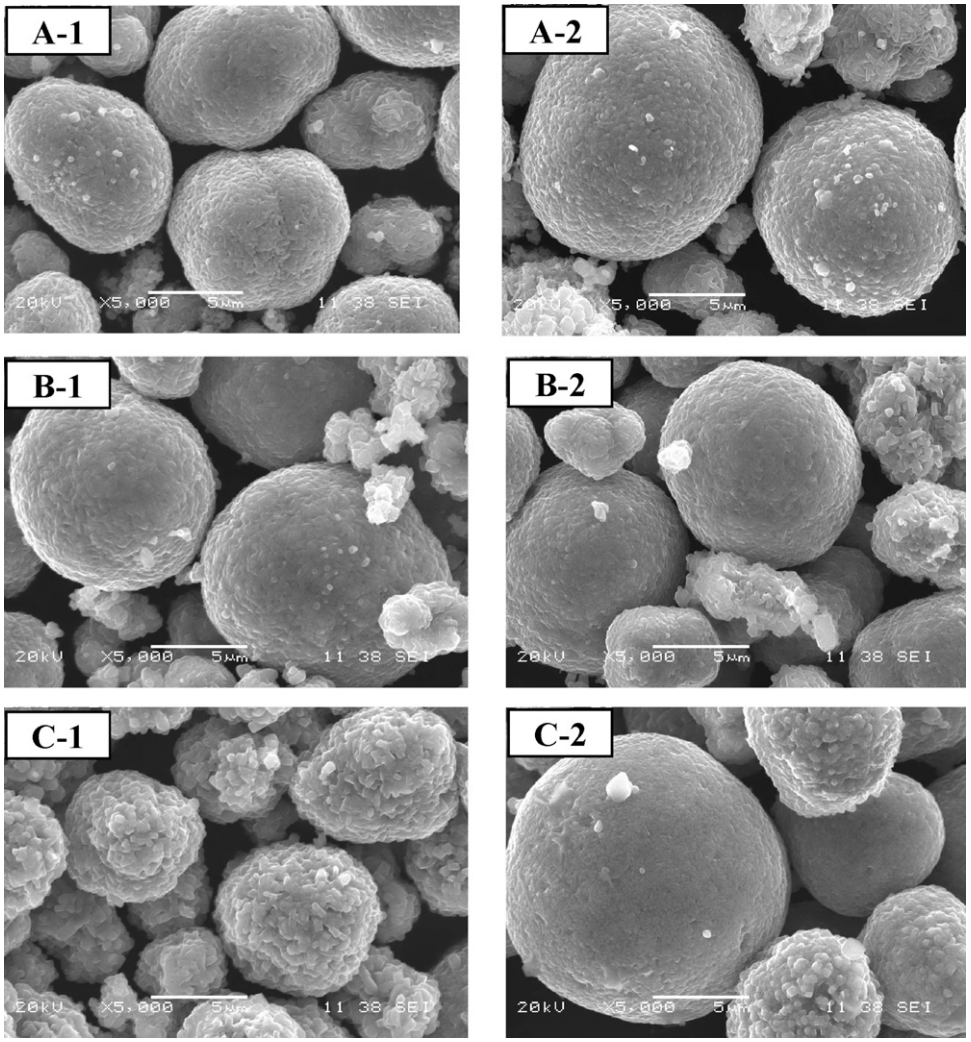

Fig. 2. Scanning electron microcopy (SEM) of Co-doped $Li[Li_xMn_{0.65*0.995(1-x)}Ni_{0.35*0.995(1-x)}Co_{0.005(1-x)}]O_2$ and non-doped $Li[Li_xMn_{0.65(1-x)}Ni_{0.35(1-x)}]O_2$ samples (A–C referring to samples of $x = 0.0909, 0.1667, 0.2308$; -1 and -2 referring to Co-doped and none-doped).

materials were mixed with 5% of carbon black and 5% of polyvinylidene fluoride (PVDF) in N-methyl pyrrolidinone (NMP) solvent until slurry was obtained. And then, the blended slurries were pasted onto an aluminum current collector, and the electrode was dried at 120 °C for 12 h in the air, then electrode pieces were cut to 16 mm in diameter. The test cell consisted of the positive electrode and lithium foil negative electrode separated by a porous polypropylene film, and a mol L^{-1} $LiPF_6$ in EC, EMC and DMC(1:1:1 in volume) as the electrolyte. The assembly of the cells was carried out in a dry Ar-filled gloved box. The test was carried out using an automatic galvanostatic charge–discharge unit NEWWARE battery cycler, at a current density of 20 mA g^{-1} versus Li/Li^+ electrode at room temperature. Different charge–discharge voltage ranges were also investigated, one is between 2.0 and 4.8 V for cyclic test; another is between 2.0 and 4.6 V during the first cycle, then change to 3.0–4.3 V for cyclic test.

3. Results and discussion

Fig. 1 shows the XRD patterns of the synthesized materials. All the diffraction peaks can be indexed as a layered oxide structure based on a hexagonal α-$NaFeO_2$ structure. The small diffraction peaks between 20° and 23° are characteristic peaks of Li_2MnO_3 or Li_2MnO_3-based materials. Some attributed those peaks to superlattice ordering of Li and Mn in the transition-metal layers [6,18,19]. The authenticity of "super lattice" and the transition metallic atom (Mn, Ni, Co, $Ni_{0.5}Mn_{0.5}$, etc.) exists in which way, are not confirmed yet up to now. Although all observed XRD peaks in each sample can be indexed only by monoclinic unit cell of Li_2MnO_3 (C2/m), some of main XRD peaks can overlap the peak of position from the unit cell of cubic rock-salt structure (Fm3m). No other crystalline impurity was detected, and Co-doping did not change the crystal structure either. Therefore, the materials prepared exhibit a pure phase, which can be simply represented as $Li[Li_xMn_{0.65(1-x)}Ni_{0.35(1-x)}]O_2$ or composite solid solution $xLi_2MnO_3{\cdot}(1-x)LiNi_{0.5}Mn_{0.5}O_2$.

The materials show a (0 0 3) peak at $2\theta = 18.5°$ as a main peak, and (1 0 4), (1 0 1), (0 1 5), (1 0 7), (0 1 8), (1 1 0), (1 1 3) planes observed at $2\theta = 45°$, 37°, 48.5°, 58.5°, 64.5°, 65.5°, 68.5° peaks respectively, which also clearly present the characteristic XRD peaks of the hexagonal structure. It can be found that split of (0 1 8) and (1 1 0) peaks are all obviously, implying well crystalline.

The SEM pictures of materials prepared were shown in Fig. 2. All the samples show analogy morphology with a quasi-spherical shape and 5–10 μm particle size approximately, which are comprised of agglomerates of much smaller primary particles. However, with the increasing of Li excess value *x*, the primary particle tends to grow up slightly. At the meantime, Co-doping makes the particle size grows more homogeneously. With which $Li[Li_{0.2308}Mn_{0.4975}Ni_{0.2679}Co_{0.0038}]O_2$ and $Li[Li_{0.2308}Mn_{0.5}Ni_{0.2692}]O_2$ sample distinctly behaves.

The ICP analysis indicated the molar ratio of transition metal ions to be 0.648:0.347:0.005 for Co-doped samples and 0.649:0.351 for none-doped samples. It is in good agreement with the composition of starting reactants. In the meantime, samples selected from different locations randomly for the same lot material were also been tested. The results keep according with the others, revealed that both Mn/Ni main element and Co doing element are all distribute homogeneously to some extent.

Electrochemical performances were investigated in two different voltage ranges, one is 2.0–4.8 V for high voltage, another is 2.0–4.6 V in the initial cycle for activation, then cycled in 3.0–4.3 V for applied research. The obtained electrochemical values are presented in Tables 1 and 2 correspondingly.

As other essays described, initial charge–discharge curves of $xLi_2MnO_3{\cdot}(1-x)LiMO_2$ materials are divided into four regions

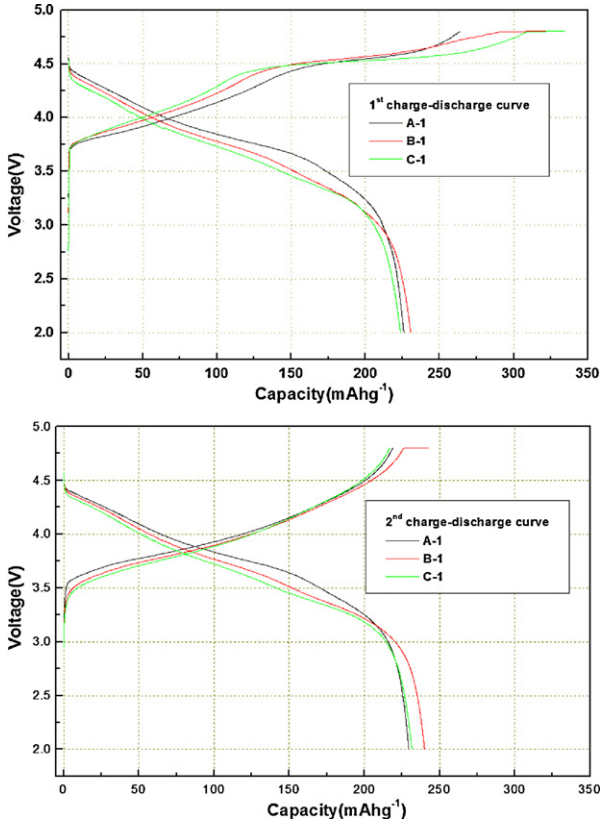

Fig. 3. Electrochemical charge/discharge profiles of Co-doped $Li[Li_xMn_{0.65*0.995(1-x)}Ni_{0.35*0.995(1-x)}Co_{0.005(1-x)}]O_2$ samples (20 mAh g^{-1}, 2.0–4.8 V) (A-1, B-1, C-1 referring to $x = 0.0909$, 0.1667, 0.2308).

(regions 1–4) as follows [12,15,20]: Li extraction by oxidation of M ion $LiMO_2$ component (<4.4 V, region 1), Li_2O extraction by oxidation of oxide ion in Li_2MnO_3 component (>4.4 V, region 2, irreversible), Li insertion by reduction of M ion (>3.5 V, region 3) and Li insertion by reduction of Mn^{4+} ion (<3.5 V, region 4).

The electrochemical performance of voltage range between 2.0 and 4.8 V were shown in Table 1, Figs. 3 and 4. It is observed that discharge capacity and initial efficiency (Q_{1d}/Q_{1c}) can be improved in certain degree through Co-doping and decreasing of Li excessive. In the meanwhile, the second efficiency (Q_{2d}/Q_{2c}) can also be improved greatly through Co-doping, which all keep the same lever of around 0.98. For none-doped samples, $Li[Li_{0.0909}Mn_{0.5909}Ni_{0.3182}]O_2$ (A-2, $x = 0.0909$) presents higher second efficiency than that of $Li[Li_{0.1667}Mn_{0.5417}Ni_{0.2917}]O_2$ (B-2, $x = 0.1667$) and $Li[Li_{0.2308}Mn_{0.5}Ni_{0.2692}]O_2$ (C-2, $x = 0.2308$), and the later two samples keep the same lever of around 0.80. However, compared to $LiCoO_2$, $LiNi_{1/3}Mn_{1/3}Co_{1/3}$, $LiNi_{0.5}Mn_{0.5}O_2$ and other layered $LiMO_2$ materials, the as prepared materials exhibit relative lower initial efficiency. The high voltage plateau of 4.5 V also exists during the initial charge and then disappears from 2nd cycle, which can be explained by irreversible Li_2O extraction of region 2 as above text mentioned. The $Li[Li_{0.0909}Mn_{0.588}Ni_{0.3166}Co_{0.0045}]O_2$ sample (A-1, $x = 0.0909$, Co-doped) expresses highest initial efficiency of 78.8% and highest energy density of 858.4 mWh g^{-1}, while the $Li[Li_{0.2308}Mn_{0.5}Ni_{0.2692}]O_2$ sample (C-2, $x = 0.2308$, none-doped) behaves lowest of 56.5% and 590.1 mWh g^{-1}. Tabuchi et al. investigated on $Li_{1+x}(Fe_yMn_{1-y})_{1-x}O_2$ materials, from which much higher density of 761–971 mWh g^{-1} can be achieved, but poorer in initial efficiency and cycle ability [5].

For Li_2MnO_3 or Li_2MnO_3-based materials, the initial discharge capacity is greatly influenced by efficiency in general. The $Li[Li_{0.1667}Mn_{0.5389}Ni_{0.2902}Co_{0.0042}]O_2$ sample (B-1, $x = 0.1667$,

Table 1
Electrochemical characteristics of Co-doped $Li[Li_xMn_{0.65*0.995(1-x)}Ni_{0.35*0.995(1-x)}Co_{0.005(1-x)}]O_2$ and non-doped $Li[Li_xMn_{0.65(1-x)}Ni_{0.35(1-x)}]O_2$ samples (A, B, C referring to samples of $x = 0.0909$, 0.1667, 0.2308; -1 and -2 referring to Co-doped and none-doped).

Sample	Q_{1d} (mAh g^{-1})	Q_{1d}/Q_{1c}	V_{ave} (V)	$V_{ave} \cdot Q_{1d}$ (mWh g^{-1})	Q_{2d} (mAh g^{-1})	Q_{2d}/Q_{2c}	Q_{30d} (mAh g^{-1})	Q_{30d}/Q_{1d}
A-1	225.9	0.788	3.80	858.4	229.5	0.974	226.0	1.000
A-2	217.2	0.744	3.77	818.4	226.0	0.862	223.2	1.028
B-1	230.5	0.714	3.71	855.2	240.1	0.987	234.9	1.019
B-2	199.3	0.673	3.73	743.8	217.1	0.799	224.1	1.124
C-1	223.7	0.668	3.67	821.0	231.6	0.987	230.9	1.032
C-2	155.7	0.565	3.79	590.1	173.1	0.804	229.8	1.476

Table 2
Electrochemical characteristics of Co-doped $Li[Li_xMn_{0.65*0.995(1-x)}Ni_{0.35*0.995(1-x)}Co_{0.005(1-x)}]O_2$ and non-doped $Li[Li_xMn_{0.65(1-x)}Ni_{0.35(1-x)}]O_2$ samples (20 mAh g^{-1}, 1st cycle: 2.0–4.6 V, from 2nd cycle: 3.0–4.3 V) (A, B, C referring to samples of $x = 0.0909$, 0.1667, 0.2308; -1 and -2 referring to Co-doped and none-doped).

Sample	Q_{1d} (mAh g^{-1})	Q_{1d}/Q_{1c}	Q_{2d} (mAh g^{-1})	Q_{2d}/Q_{2c}	V_{ave} (V)	$V_{ave} \cdot Q_{1d}$ (mWh g^{-1})	Q_{31d} (mAh g^{-1})	Q_{31d}/Q_{2d}
A-1	200.0	0.783	150.2	0.920	3.83	575.3	152.4	1.015
A-2	190.7	0.740	147.9	0.841	3.81	563.8	147.6	0.998
B-1	168.8	0.669	130.0	0.917	3.82	496.6	140.1	1.078
B-2	150.0	0.645	115.2	0.767	3.82	440.1	120.4	1.045
C-1	186.9	0.650	143.8	0.926	3.77	542.1	145.1	1.009
C-2	100.4	0.578	74.3	0.760	3.86	287.0	87.1	1.172

Co-doped) shows the highest discharge capacity, 230.5 mAh g^{-1}, while the other two Co-doped samples vary in 225.9 and 223.7 mAh g^{-1} respectively. On the other hand, Li excess value x between 0.0909 and 0.1667 of none-doped samples present the discharge capacity of 217.2, 199.3, 155.7 mAh g^{-1}, decreasing with the increase of Li content. It is supposed that with the increasing of Li excess, the proportion of Li_2MnO_3 in solid solution $xLi_2MnO_3 \cdot (1-x)LiMO_2$ also increases, thus conduction of lithium ion, initial efficiency and initial discharge capacity are affected altogether. The trend is also in accordance with the variation of charge–discharge voltage plateau, which can further confirm the proportion change in solid solution. The voltage plateau variation trend of Co-doped samples is similar to that of none-doped. With the increasing of Li_2MnO_3 proportion, Li insertion by reduction of Mn^{4+} ion (<3.5 V, region 4) increases and Li insertion by reduction of M ion (>3.5 V, region 3) decreases correspondingly, resulted in descending of voltage plateau. Therefore, distinct voltage plateau variation from 3.6 V to 3.8 V for different samples is observed. Furthermore, Li ion diffusion is enhanced in certain degree after

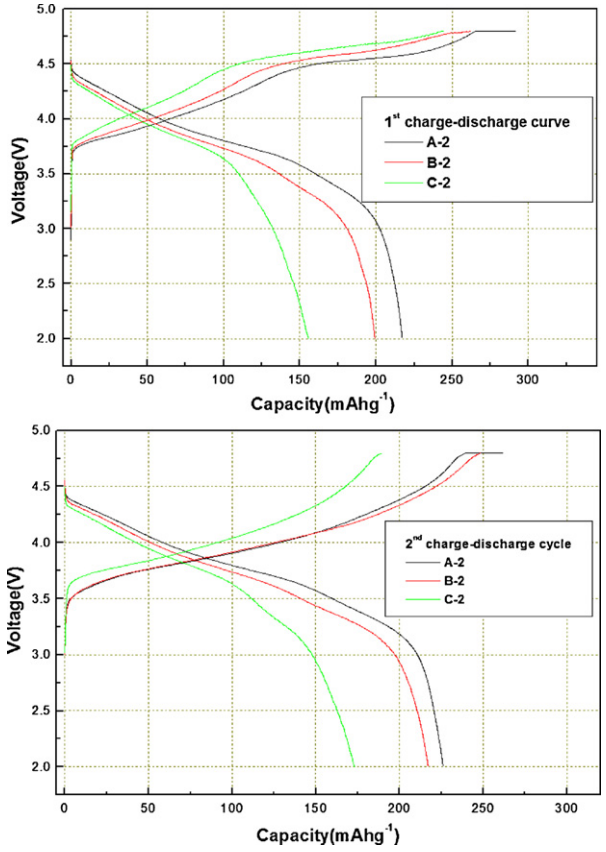

Fig. 4. Electrochemical charge/discharge profiles of non-doped $Li[Li_xMn_{0.65(1-x)}Ni_{0.35(1-x)}]O_2$ samples (20 mAh g^{-1}, 2.0–4.8 V) (A-2, B-2, C-2 referring to $x = 0.0909$, 0.1667, 0.2308).

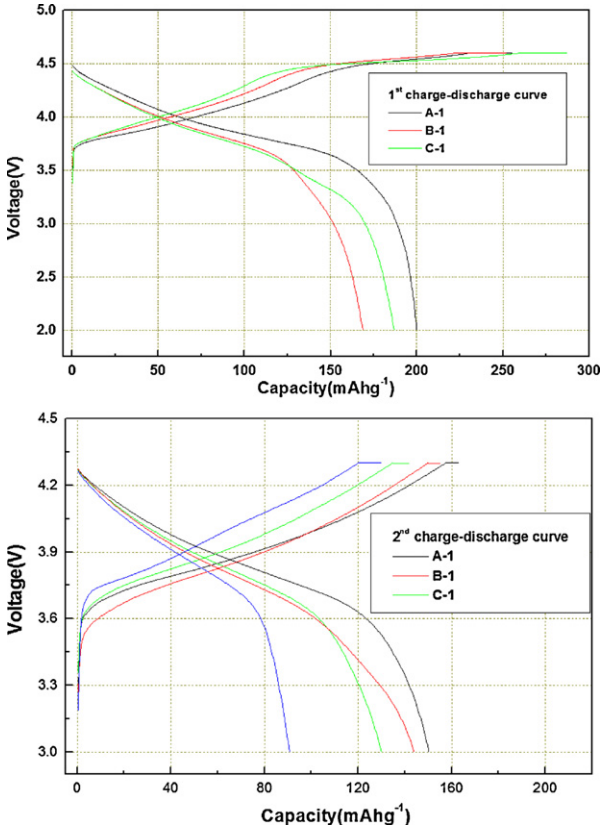

Fig. 5. Electrochemical charge/discharge profiles of Co-doped $Li[Li_xMn_{0.65*0.995(1-x)}Ni_{0.35*0.995(1-x)}Co_{0.005(1-x)}]O_2$ samples (20 mAh g^{-1}, 1st cycle: 2.0–4.6 V, 2nd cycle: 3.0–4.3 V) (A-1, B-1, C-1 referring to $x = 0.0909$, 0.1667, 0.2308).

Co-doping, while $Li[Li_{0.2308}Mn_{0.5}Ni_{0.2692}]O_2$ sample (C-2, $x = 0.2308$, none-doped) displays lowest capacity in both region 3 and region 4 thus steep drop below 3.6 V in charge–discharge curves also occurred. For different none-doped samples, discharge capacity varies greatly from Li excess value of 0.0909 to 0.2308, whereas Co-doped samples keep the same higher lever.

Table 2, Figs. 5 and 6 present the electrochemical performance of following voltage range: 1st cycle: 2.0–4.6 V, from 2nd for cyclic test: 3.0–4.3 V. The $Li[Li_{0.0909}Mn_{0.588}Ni_{0.3166}Co_{0.0045}]O_2$ sample expresses highest initial efficiency of 78.3%, while the $Li[Li_{0.2308}Mn_{0.5}Ni_{0.2692}]O_2$ sample behaves lowest of 57.8%. The discharge capacity varies from 200.0 to 100.4 mAh g^{-1} (Q_{1d}) in initial charge–discharge of 2.0–4.6 V, and from 150.2 to 74.3 mAh g^{-1} (Q_{2d}) in the second cycle of 3.0–4.3 V. The variation trend of initial efficiency (Q_{1d}/Q_{1c}), the second efficiency (Q_{2d}/Q_{2c}), discharge capacity, voltage plateau, etc., are in accordance with charge–discharge between 2.0 and 4.8 V. However, for Co-doped samples, it can be found that the discharge capacity in initial 2.0–4.6 V vary greatly for different Li excess samples. The trend is different from 2.0 to 4.8 V, the discharge of which almost keeps the same. It reveals that in relative lower voltage, the extraction and insertion of Li ion tends to more easily when Li excessive keeps lower.

The cycle ability in different charge–discharge voltage ranges is presented in Figs. 7 and 8. At the initial stage of cycle process, it is observed that capacity keeps on going up significantly, especially in the voltage range of 2.0–4.8 V. It can reach to the highest discharge capacity approximately in the fifth cycle. Furthermore, almost no reduction is observed after 30 times cycle in 3.0–4.3 V range. Compared to $LiCoO_2$, $Li(Ni_{1/3}Mn_{1/3}Co_{1/3})O_2$ and other cathode materials, the as prepared materials present both

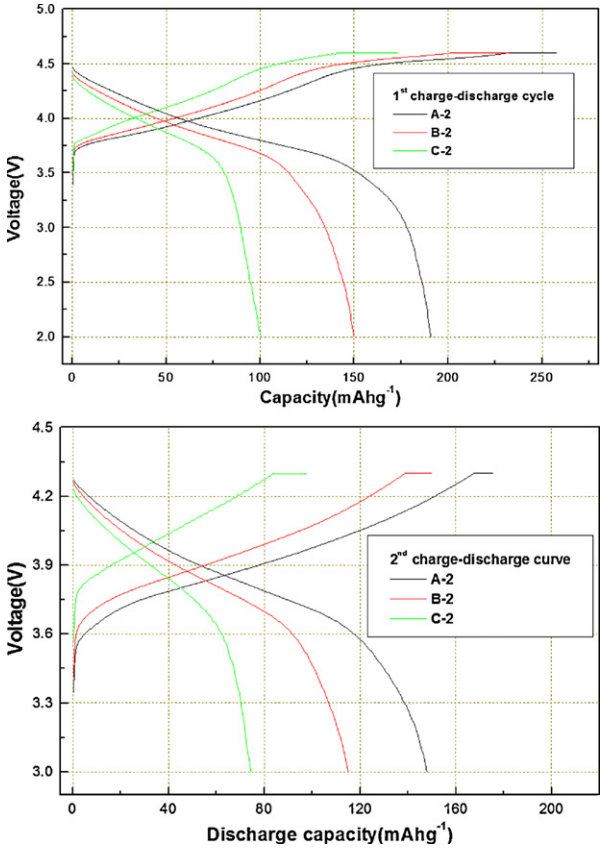

Fig. 6. Electrochemical charge/discharge profiles of non-doped $Li[Li_xMn_{0.65(1-x)}Ni_{0.35(1-x)}]O_2$ samples (20 mAh g^{-1}, 1st cycle: 2.0–4.6 V, 2nd cycle: 3.0–4.3 V) (A-2, B-2, C-2 referring to $x = 0.0909$, 0.1667, 0.2308).

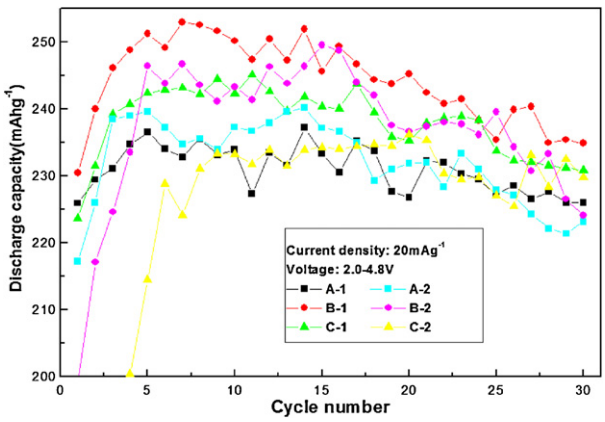

Fig. 7. Cycle performance of Co-doped $Li[Li_xMn_{0.65*0.995(1-x)}Ni_{0.35*0.995(1-x)}Co_{0.005(1-x)}]O_2$ and non-doped $Li[Li_xMn_{0.65(1-x)}Ni_{0.35(1-x)}]O_2$ samples (A, B, C referring to samples of $x = 0.0909$, 0.1667, 0.2308; -1 and -2 referring to Co-doped and none-doped).

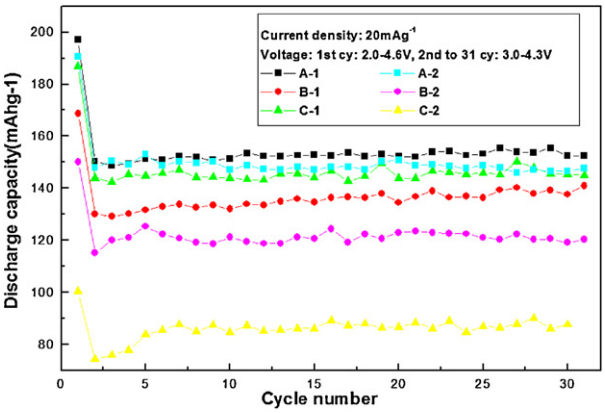

Fig. 8. Cycle performance of Co-doped $Li[Li_xMn_{0.65*0.995(1-x)}Ni_{0.35*0.995(1-x)}Co_{0.005(1-x)}]O_2$ and non-doped $Li[Li_xMn_{0.65(1-x)}Ni_{0.35(1-x)}]O_2$ samples (20 mAh g^{-1}, 1st cycle: 2.0–4.6 V, from 2nd cycle: 3.0–4.3 V) (A, B, C referring to samples of $x = 0.0909$, 0.1667, 0.2308; -1 and -2 referring to Co-doped and none-doped).

excellent discharge capacity and excellent cycle performance. It can be explained by well solid solution of $Li(Ni_{0.5}Mn_{0.5})O_2$ and Li_2MnO_3, among which the former provides high capacity, the later ensures structure and cycle stability. Yabubuchi et al. viewed that high capacity of the Li-rich Mn-based materials after the first charge to high voltage is constituted of redox reaction of Mn^{3+}/Mn^{4+} and oxygen reduction at the electrode surface [21]. In the voltage range of 2.0–4.6 V, $Li[Li_{0.0909}Mn_{0.588}Ni_{0.3166}Co_{0.0045}]O_2$ sample behaves highest in discharge capacity and initial efficiency. However, in the 2.0–4.8 V, despite of the initial discharge capacity is greatly improved through Co-doping process; the highest capacity and capacity retention almost keep in the same lever for the same ratio Li/Me samples. The $Li[Li_{0.1667}Mn_{0.5389}Ni_{0.2902}Co_{0.0042}]O_2$ sample exhibit the relative higher discharge capacity of 252.0 mAh g^{-1} during cyclic test.

4. Conclusions

Li-rich Mn-based Co-doped $Li[Li_xMn_{0.65*0.995(1-x)}Ni_{0.35*0.995(1-x)}Co_{0.005(1-x)}]O_2$ and none-doped $Li[Li_xMn_{0.65(1-x)}Ni_{0.35(1-x)}]O_2$ cathode materials were prepared by a conventional solid-state reaction. Li excess value x of 0.0909, 0.1667 and 0.2308 were selected and pure phase can be obtained. With the increasing of Li excessive, the primary particle tends to grow up slightly. Co-doping makes the particle size grows more homogeneously. ICP analysis indicated the as prepared materials are in good agreement

with the composition of starting reactants. The initial efficiency (Q_{1d}/Q_{1c}) and the second efficiency (Q_{2d}/Q_{2c}) can be improved in certain degree through Co-doping and optimization of mole ratio Li/Me. The $Li[Li_{0.0909}Mn_{0.588}Ni_{0.3166}Co_{0.0045}]O_2$ sample expresses highest initial efficiency of 78.8% and highest energy density of 858.4 mWh g^{-1}, while the $Li[Li_{0.2308}Mn_{0.5}Ni_{0.2692}]O_2$ sample behaves lowest of 56.5% and 590.1 mWh g^{-1}. The discharge capacity of Co-doped samples behave between 220 and 230 mAh g^{-1} in 2.0–4.8 V, while none-doped samples present 217.2, 199.3, 155.7 mAh g^{-1} correspondingly. Electrochemical performances were also checked up in different voltage ranges for applied research. For Co-doped samples, capacity varies greatly when test carried out in initial voltage of 2.0–4.6 V. Almost no capacity loss is observed after 30 cycles. The as prepared materials display both high discharge capacity and excellent cycle performance.

References

[1] C.S. Johnson, J.-S. Kim, C. Lefief, N. Li, J.T. Vaughey, M.M. Thackeray, Electrochemistry Communications 6 (2004) 1085.
[2] S.-H. Park, Y. Sato, Y.-K. Kim, Y.-S. Lee, Materials Chemistry Physics 102 (2007) 225.
[3] Y. Koyama, I. Tanaka, M. Nagao, R. Kanno, Journal of Power Sources 189 (2009) 798.
[4] A. Boulineau, L. Croguennec, C. Delmas, F. Weill, Solid State Ionics 180 (2010) 1652.
[5] M. Tabuchi, Y. Nabeshima, T. Takeuchi, K. Tatsumi, J. Imaizumi, Y. Nitta, Journal of Power Sources 195 (2010) 834.
[6] K.S. Park, M.H. Cho, S.J. Jin, C.H. Song, K.S. Nahm, Journal of Power Sources 146 (2005) 281.
[7] P.S. Whitfield, S. Niketic, I.J. Davidson, Journal of Power Sources 146 (2005) 617.
[8] S.H. Kim, S.J. Kim, K.S. Nahm, H.T. Chung, Y.S. Lee, J. Kim, Journal of Alloys and Compounds 449 (2008) 339.
[9] X.-J. Guo, Y.-X. Li, M. Zheng, J.-M. Zheng, J. Li, Z.-L. Gong, Y. Yang, Journal of Power Sources 184 (2008) 414.
[10] L. Yu, W. Qiu, F. Lian, W. Liu, X. Kang, J. Huang, Materials 62 (2008) 3010.
[11] L. Yu, W. Qiu, F. Liana, J. Huang, X. Kang, Journal of Alloys and Compounds 471 (2009) 317.
[12] J.-H. Lim, H. Bang, K.-S. Lee, K. Amine, Y.-K. Sun, Journal of Power Sources 189 (2009) 571.
[13] Y. Wu, A. Manthiram, Journal of Power Sources 183 (2008) 749.
[14] Y. Wu, A. Manthiram, Solid State Ionics 180 (2009) 50.
[15] S.-H. Kang, M.M. Thackeray, Electrochemistry Communications 11 (2009) 748.
[16] A. Ito, D. Li, Y. Sato, M. Arao, M. Watanabe, M. Hatano, H. Horiea, Y. Ohsawa, Journal of Power Sources 195 (2010) 567.
[17] R. Santhanam, P. Jones, A. Sumana, B. Rambabu, Journal of Power Sources 195 (2010) 7391.
[18] P. Strobel, B. Lambert Andron, Journal of Solid State Chemistry 75 (1) (1988) 90.
[19] Y. Shin, A. Manthirm, Electrochimica Acta 48 (2003) 3583.
[20] M. Tabuchi, Y. Nabeshima, T. Takeuchi, H. Kageyama, K. Tatsumi, J. Akimoto, H. Shibuya, J. Imaizumi, Journal of Power Sources 196 (2011) 3611.
[21] N. Yabubuchi, K. Yoshii, S.-T. Myung, I. Nakai, S. Komaba, Journal of the American Chemical Society 133 (2011) 4404.